

## Article

# Oxyfluorides of Rare-Earth Elements in the Rocks of the Shatak Formation (Southern Urals)

Sergey G. Kovalev \*, Sergey S. Kovalev and Aysylu A. Sharipova 

Institute of Geology, Ufa Federal Research Centre, Russian Academy of Sciences, Karl Marx Street, 16/2, 450077 Ufa, Russia; aysyluazatovna@mail.ru (A.A.S.)

\* Correspondence: kovalev@ufaras.ru

**Abstract:** The Shatak Formation, comprising a part of the Mashak Suite (RF<sub>2</sub>), is located on the western slope of the Southern Urals. It consists of various rock types, including sedimentary rocks, such as conglomerates, polymictic sandstones, aleurolites, and carbonaceous clayey shales, as well as igneous rocks, including picrites, basalts, dacites, rhyodacites, and rhyolites, and volcanogenic–sedimentary rocks, such as tuffs and tuff breccias. In this article, oxyfluoride (La, Ce) (O<sub>n</sub>F<sub>m</sub>)<sub>3</sub> mineralization, occurring in the contact zone between the metabasalts and quartz sandstones, is described for the first time in the literature. This is represented by compounds of variable compositions forming an isomorphic series: trifluoride, (La, Ce)F<sub>3</sub>–oxyfluoride, (La, Ce)OF–oxide, and (La, Ce)<sub>2</sub>O<sub>3</sub>. By analyzing several binary phase diagrams, significant coordination between oxygen, fluorine, and cerium in the chemical composition of oxyfluorides has been highlighted. However, the behavior of lanthanum has been shown to exhibit some irregularity. The genesis of oxyfluoride mineralization is attributed to the regional metamorphism of rocks within the Shatak Formation. During the hydrothermal process, the decomposition of fluorapatite, which is unstable during both hydrothermal metamorphism and supergene processes, resulted in the release of fluorine, as well as potentially lanthanum and cerium. Variations in the chemical composition of oxyfluorides, which are formed in the presence of an excess of oxygen resulting from water dissociation, are determined by local differences in the content of the main components within the forming microfractures.

**Keywords:** Southern Urals; Shatak Formation; regional metamorphism; rare-earth elements; oxyfluorides



**Citation:** Kovalev, S.G.; Kovalev, S.S.; Sharipova, A.A. Oxyfluorides of Rare-Earth Elements in the Rocks of the Shatak Formation (Southern Urals). *Minerals* **2023**, *13*, 935. <https://doi.org/10.3390/min13070935>

Academic Editor: Vysetti Balaram

Received: 30 May 2023

Revised: 5 July 2023

Accepted: 11 July 2023

Published: 13 July 2023



**Copyright:** © 2023 by the authors. Licensee MDPI, Basel, Switzerland. This article is an open access article distributed under the terms and conditions of the Creative Commons Attribution (CC BY) license (<https://creativecommons.org/licenses/by/4.0/>).

## 1. Introduction

Rare-earth elements (REEs) and their compounds have found widespread use across many industrial applications, particularly in the production of composite materials. REE compounds play a crucial role as alloying or modifying additives, effectively enhancing strength properties, broadening operational temperature ranges, and imparting other desirable material characteristics.

Despite their importance, the mineralogy of REE fluorides has received limited attention due to their relatively uncommon occurrence in nature. Trifluorides, such as fluocerite-(Ce) and fluocerite-(La), as well as fluorocarbonates, like bastnaesite, synchysite, and parasite, are known examples of REE fluoride minerals. Although rare, fluocerite has been extensively documented in numerous publications worldwide [1–13]. Often found in rare-metal granites, pegmatites, and rare-metal greisen formations, fluocerite, which predominantly occurs as a rare earth oxyfluoride rather than in its pure form as a neutral trifluoride, exhibits a characteristic defect structure [2,14,15]. Although holleniuzite-(La) is the only mineral that has been identified as an inherent oxyfluoride [16], in 2021, a newly discovered mineral called holleniuzite-(Ce) was officially recognized by the International Mineralogical Association (IMA). This new mineral was named after the discovery of cerium oxyfluoride in volcanic ejecta from the Agua de Pau volcano on São Miguel Island in the Azores [17].

The Shatak Complex is part of the Mashak Formation, which includes the Middle-Riphean section of the stratotypic Riphean sequence in Northern Eurasia. Despite a significant number of publications dedicated to the geological structure, lithology, and petrography of the complex, as well as various topics related to its stratigraphy, geochemistry, and mineralogy [18–25], many issues either remain subject to debate, or have been overlooked or almost ignored in the contemporary literature.

The present study focuses on the characterization of a previously unidentified mineralization occurrence in the rocks of the Shatak Formation located in the Southern Urals, Russia. This newly discovered mineralization type comprises oxyfluorides of the rare-earth elements, specifically (La, Ce).

## 2. Geological Setting

The Shatak Formation is situated in the Bashkir Meganticlinorium comprising part of the Mashak Suite. It is located beneath the Middle Riphean deposits of the Riphean stratotype section (Figure 1). The age of these rocks in the Middle Riphean was determined using the zircon-dating methods on basaltoids. The CA-TIMS (CA-ID-TIMS) method provided the ages of  $1380.6 \pm 1.1$  Ma for the  $^{207}\text{Pb}/^{206}\text{Pb}$  ratio and  $1380.1 \pm 0.5$  Ma for the  $^{206}\text{Pb}/^{238}\text{U}$  ratio [26], respectively.

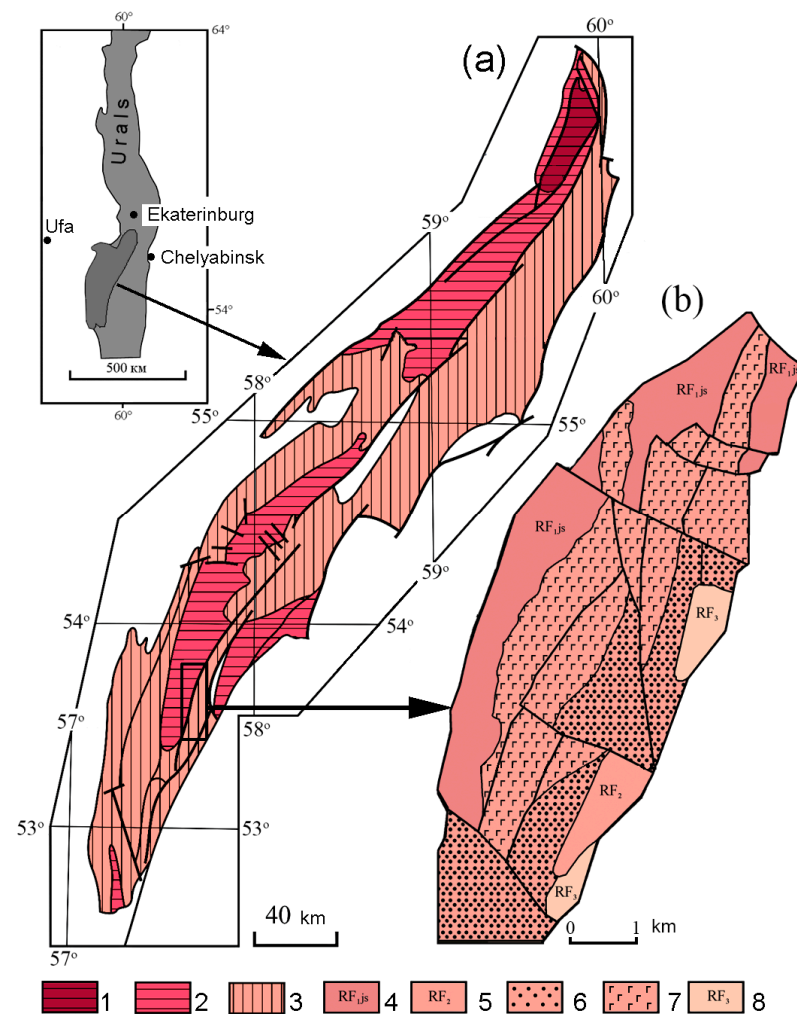


**Figure 1.** (a) Geological scheme of the Bashkirian Anticlinorium. (b) Geological map of the Shatak Complex. 1—Archean–Paleoproterozoic sediments not dissected; 2—Lower Riphean sediments; 3—Middle Riphean sediments; 4—Jusha Formation; 5—non-dissected deposits of the Zigazino–Komarovsk and Avzyan Formations; 6—Zigalga Formation; 7—Mashak Formation; and 8—Upper Riphean.

In terms of its structure, the complex is found on the eastern flank of the Yamantau anticlinorium and forms a monoclinical structure with disjunctive faults and minor folding. The deposits of the complex, which overlay the Lower Riphean Yushino Suite, are followed by Zigalga quartz sandstones and quartzite sandstones. The Mashak Suite, represented by the Bolshoi Shatak mountain range, comprises sedimentary rocks (conglomerates, polymictic sandstones, aleurolites, and carbonaceous clayey shales), igneous rocks (picrites, basalts, dacites, rhyodacites, and rhyolites), and volcanogenic–sedimentary rocks (tuffs and tuff breccias).

Sedimentary rocks of the complex, which make up about 75% of its volume, are mainly represented by conglomerates and sandstones. Siltstones and clay shales are relatively rare. Conglomerates are developed at several stratigraphic levels. These are primarily composed of well-rounded fragments of quartzite sandstones and quartzites, accounting for 70%–80% of its content, and less often ferruginous quartzite sandstones and microquartzites. The cement consists of a quartzitic sandstone material and a finely-flaked sericite–chlorite mass. Sandstones are represented by quartzitic variations, of which 80%–90% consist of quartz fragments with chlorite–sericite cement. Aleurolites, siltstones, and clay shales occur in a thin interlayer with each other, less frequently forming independent thin horizons and bundles.

Basalts comprise medium-fine-grained rocks characterized by microdoleritic, microphytic, apointersertal, and porphyritic structures. The mineral composition includes: clinopyroxene, plagioclase, amphibole, titanomagnetite, and magnetite. These rocks are largely metamorphosed, with the association of secondary minerals being represented by amphibole (actinolite), muscovite, chlorite, epidote, sericite, titanite, and leucoxene. Their maximum number is fixed in the Kuz’elga (lower) and Karansky (upper) sub-suites.

The acidic varieties of rocks are represented by dacites, rhyodacites, and rhyolites. Dacites and rhyodacites are light gray rocks of a fine-medium-grained, porphyritic structure having a massive texture. The mineral composition includes: amphibole (rarely), plagioclase (albite), quartz, sericite, chlorite, biotite, ore mineral, titanite, and leucoxene. Rare amphibole crystals are pseudomorphically replaced by a carbonate–sericite–chlorite association. The bulk of these rocks are composed of small grains of quartz, chlorite, and biotite. Rhyolites are light gray rocks with porphyritic fluid and a schlier-taxitic structure. The bulk is composed of a fine-grained quartz aggregate. Albite occurs in porphyritic secretions. Dark-colored minerals are represented by greenish-brown biotite and chlorite. Apatite, allanite, titanite, and magnetite are typically found as accessory minerals.

The diverse chemical composition of the rocks of the Shatak Complex varies from alkaline varieties (trachybasalts and trachydacites) to low-alkaline picrobasalts, basalts, and rhyolites (Figure 2a).

Basaltoids exhibit geochemical characteristics that indicate its enrichment in the light rare-earth element (LREE). The basalts of the Kuz’elga sub-formation group have  $La_n/Lu_n$  ratios ranging from 3.56 to 6.21, and  $Ce_n/Yb_n$  ratios ranging from 3.04 to 4.83, respectively. For the basalts of the Karansky sub-formation, the  $La_n/Lu_n$  ratios range from 0.91 to 4.42, and the  $Ce_n/Yb_n$  ratios range from 0.48 to 3.58, respectively. Additionally, there is significant fractionation within the light lanthanides themselves, with  $La_n/Sm_n$  ratios from 1.73 to 2.89 for the basalts of the Kuz’elga sub-formation, and from 0.6 to 2.29 for the Karansky sub-formation, respectively (as shown in Figure 2b). Most of the rhyolites in the complex exhibit a potassic specialization, with  $K_2O/Na_2O$  ratios ranging from 0.32 to 18.52, respectively. The distribution of rare-earth elements within the rhyolites also displays a significant differentiation (Figure 2b). The degree of REE fractionation varies widely, with  $La_n/Lu_n$  ratios ranging from 3.55 to 12.89 (reaching a maximum of 112.23), and  $Ce_n/Yb_n$  ratios ranging from 2.07 to 6.39 (reaching a maximum of 66.09), respectively. At the same time, the fractionation of the light group ( $La_n/Sm_n$ ) ranges from 3.33 to 4.61, and the fractionation of heavy group ( $Gd_n/Yb_n$ ) ranges from 0.79 to 1.44 (up to a maximum of 9.53), respectively.

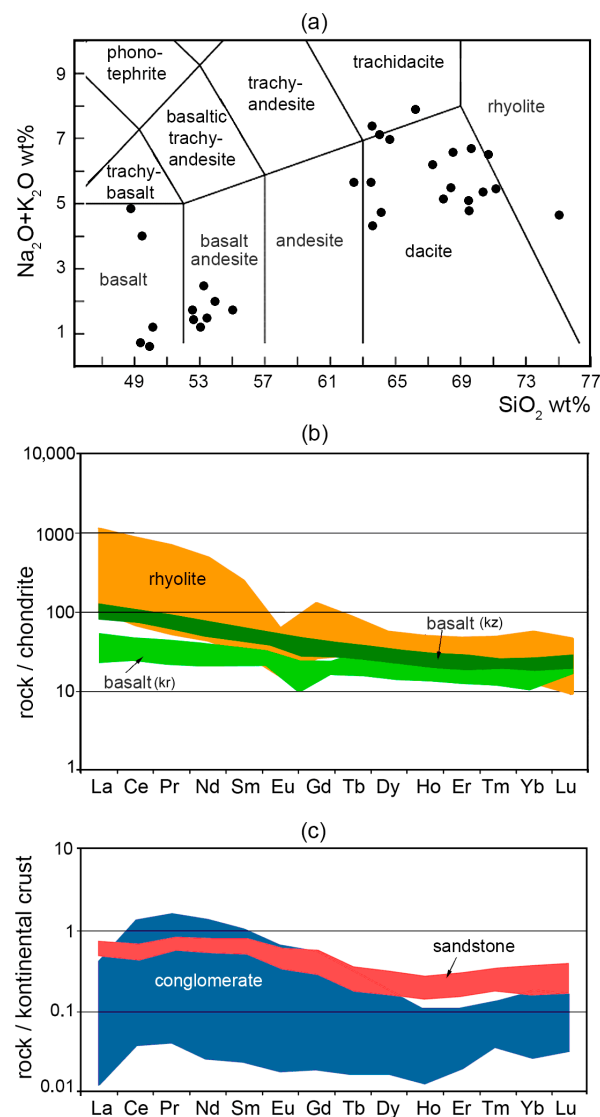


**Figure 2.** Classification diagram of  $\text{SiO}_2$ – $\text{Na}_2\text{O} + \text{K}_2\text{O}$  (a) and normalized REE distribution for igneous (b) and terrigenous (c) rocks of the Shatak Complex. Primitive mantle according to [27]. Continental crust according to [28].

The distribution of REE in the Shatak Complex conglomerates exhibits a wide range of values, spanning two orders of magnitude for the entire REE group. Despite this wide spread, the trends observed among the samples are almost identical (Figure 2c). We attribute this similarity to the variable amount of quartz pebble material present in these samples. On the other hand, the degree of REE fractionation displays a significant variation. The  $\text{La}_n/\text{Lu}_n$  ratio ranges from 0.12 to 2.87, while the  $\text{Ce}_n/\text{Yb}_n$  ratio ranges from 0.55 to 10.89, respectively. Additionally, a differentiation is observed in both the of light REE ( $\text{La}_n/\text{Sm}_n$  ratio: 0.17–1.13) and heavy REE ( $\text{Gd}_n/\text{Yb}_n$  ratio: 0.4–4.51) groups. The normalized distribution of REE in sandstones exhibits a trend configuration similar to that of the conglomerates (see Figure 2c), but with a much smaller range of values. The degree of fractionation remains within narrower limits, with  $\text{La}_n/\text{Lu}_n$  ranging from 1.82 to 2.9, and  $\text{Ce}_n/\text{Yb}_n$  ranging from 1.89 to 2.71, respectively. Furthermore, the differentiation observed in the light REE ( $\text{La}_n/\text{Sm}_n$  ratio: 0.89–0.93) and heavy REE ( $\text{Gd}_n/\text{Yb}_n$  ratio: 1.57–1.77) groups is also relatively constrained.

Recent studies on the mineralogy of magmatic and terrigenous rocks within the Shatak Formation have revealed the presence of numerous rare-earth element (REE) minerals. These include allanite-(Ce), monazite-(Ce), monazite-(La), monazite-(Nd), nioboeshinite-

(Y), eshinite-(Y), thalenite-(Nd), thalenite-(Dy), synchysite-(Ce), and Ce–La–Fe oxide, as well as previously unidentified compounds, such as yttrium silicate, cerium silicate, Ce–Fe compounds, and REE-containing minerals, like epidote, fluorapatite, and rhodochrosite.

The investigated area focuses on the contact zone between the metabasalts and terrigenous rocks of the lower Kuz’elga sub-formation within the Mashak Suite (Figure 3a). It is noteworthy in that the basalts in this region have undergone significant metamorphism. The preserved structure exhibits porphyritic, intersertal, and massive textures. The porphyritic portions mainly consist of plagioclase and clinopyroxene, which have been largely replaced by chlorite–sericite–epidote assemblages with varying mineral concentrations.

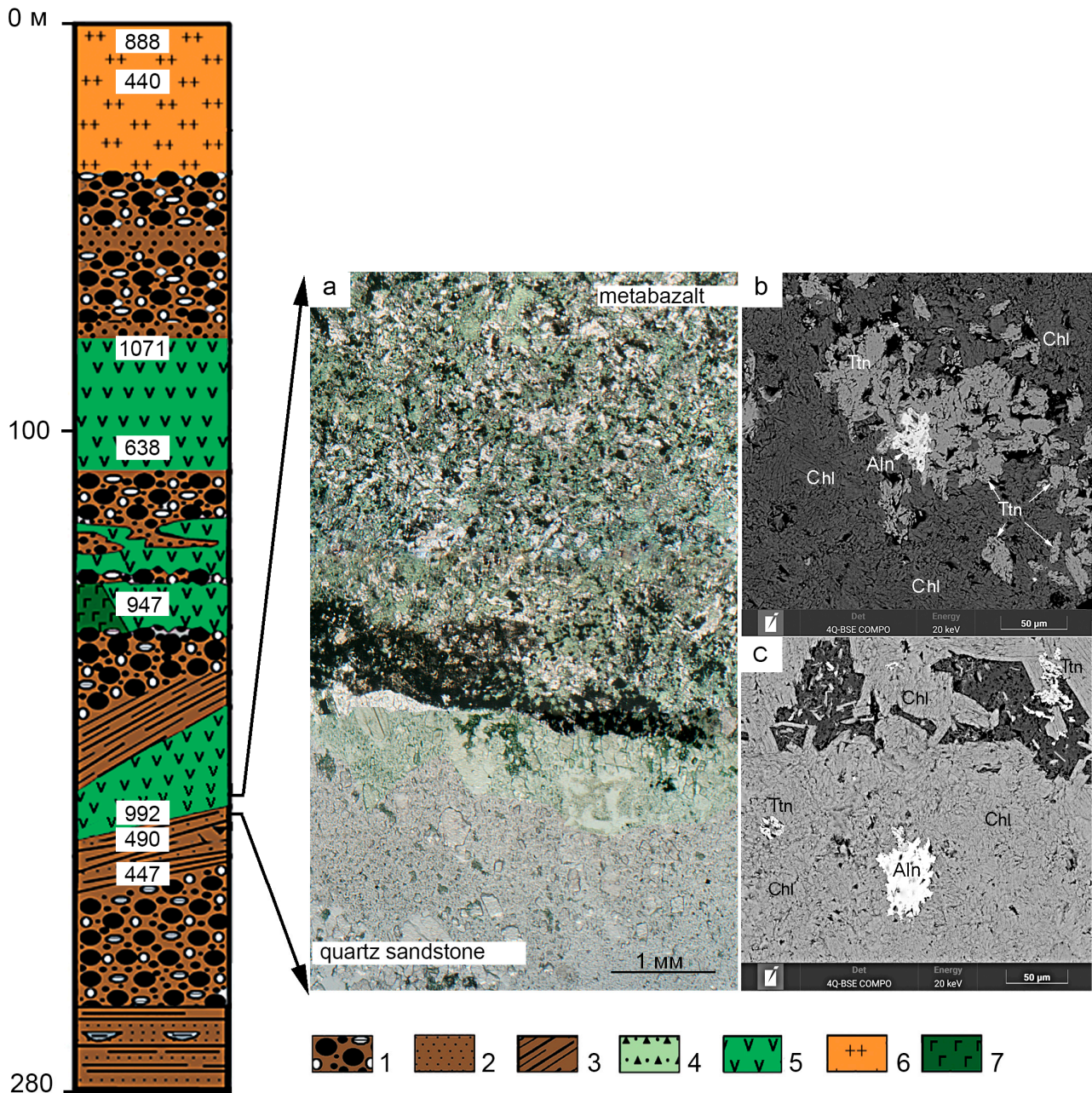


**Figure 3.** (a) Section of the Kuz’elga sub-formation showing the contact zone between the metabasalts and the quartz sandstones, along with micrographs. (b) Mineral composition of the contact zone. (c) Mineral composition of the contact zone. The numbers on the diagram indicate the fluorine content (ppm). 1—conglomerates; 2—sandstones; 3—shales; 4—tuffs, tuff sandstones; 5—metabasalts; 6—rhyolites; and 7—dolerites. Aln—allanite; Chl—chlorite; and Ttn—titanite.

The groundmass of the rocks primarily consists of plagioclase laths in various orientations, along with clinopyroxene grains partially replaced by epidotes and chlorites. In addition, devitrified rock glass can also be observed, along with ore minerals, such as magnetite and leucoxenized titanomagnetite.

The quartz sandstone, which exhibits a psammite structure and a layered texture, is composed of unrounded and semi-rounded clasts cemented by chlorite basal cement. Other less common fragments present include microquartzites, shales, and ferruginized rocks with undefined compositions. Auxiliary minerals found in the rock include zircon, tourmaline, glauconite, and various ore minerals. The immediate contact zone is characterized by chlorites that contain quartz–chlorite microbudins. In addition to chlorite and quartz, this zone also contains fluorapatite, xenomorphic allanite segregations, titanite aggregates, as well as carbonatization in the form of single crystals and calcite microveinlets (Figure 3b,c). Furthermore, sulfide–selenide mineralization, consisting of a chalcopyrite–bornite association with chalcocine, galena, molybdenite, betekhtinite, and greenockite, has been previously described in this zone [29].

### 3. Materials and Methods

Samples for research were taken from the contact zone between the metamorphosed basalts and quartz sandstones (a sample of metamorphosed basalt, a sample of chlorite rock from the direct contact zone, and a sample of chloritized quartz sandstone). The minerals were examined using a Tescan Vega Compact scanning electron microscope (Brno-Kohoutovice, Czech Republic), which was equipped with an Oxford Instruments Xplorer EDS detector (Oxford Instruments plc, Oxon, UK). This analysis took place at Institute of Geology of the Ural Federal Research Centre RAS, Ufa, Russia. The obtained spectra were processed automatically using the AzTec One software (Oxford Instruments plc, Oxon, UK) package with the TrueQ algorithm. The experimental conditions were set as follows: an accelerating voltage of 20 kV, a probe current of 4 nA, a spectral accumulation time of 60 s in the Point&ID mode, and a beam diameter of 3  $\mu\text{m}$ . Oxford Instruments standards, consisting of natural and synthetic compounds, were used for the analysis. Mineral formulas were determined using a previously established procedure [30,31].

Fluorine concentrations were analyzed at IG UFRC RAS in Ufa using the X-ray fluorescence method (A VRA-30 spectrometer from Carl Zeiss, Göttingen, Germany), equipped with a W-anode X-ray tube operating at 30 kV and 40 mA, was employed for this purpose. The detection limits for fluorine were determined to be 0.01%.

### 4. Results

Oxyfluorides were identified within the chlorite rocks (Figure 4). These oxyfluorides are characterized with the presence of microglobular formations of varying sizes, primarily found within elongated, xenomorphic schlier-like zones, which could be interpreted as cavities. In certain cases, this oxyfluoride material has been observed to impregnate the peripheral regions and cracks of deformed bornite, as depicted in Figure 4h. The individual oxyfluoride crystals are relatively large, ranging from 6 to 8  $\mu\text{m}$  in size. These exhibit isometric, ellipsoidal, xenomorphic, and occasionally poor dipyramidal shapes.

Among the other rare-earth elements listed in Table 1, oxyfluorides exhibit varying concentrations of lanthanum and cerium. This variability can be attributed to the ability of these ions to substitute for each other within the crystal structure, resulting in the formation of homogeneous compounds [14].

The analysis of a series of binary phase diagrams (Figure 5) revealed the interrelation between the main elements in the chemical composition of the detected oxyfluorides. A nearly ideal inverse dependence, having a coefficient of determination of  $R^2 = 0.99$  (the coefficient of determination is defined as a statistical measure that indicates the proportion of the variance in the dependent variable that can be explained by the independent variable(s) in a regression analysis) was observed between oxygen and fluorine. This characterizes the “oxidation” process of fluocerite-(La) (analysis No. 205\_1\_37, Table 1),

progressing through intermediate compounds such as (La, Ce)OF, and ultimately leading to the formation of La–Ce oxide (analysis No. 205\_1\_84, Table 1). The isomorphism between oxygen and fluorine was demonstrated by the inverse relationship between La and Ce, having a determination coefficient  $R^2 = 0.59$  (Figure 5). Additionally, the O–Ce–F plots display a direct relationship between oxygen and cerium, having a determination coefficient  $R^2 = 0.73$ , and an inverse relationship between fluorine and cerium, having a determination coefficient  $R^2 = 0.76$ . However, no significant correlations were observed between O–La–F (determination coefficient  $R^2 = 0.33$ ). Therefore, in the process of oxyfluoride formation, the strongest interrelation occurred between oxygen, fluorine, and cerium, while the behavior of lanthanum was typically unsystematic.

**Table 1.** Chemical composition (wt%) of oxyfluorides extracted from rocks of the Shatak Formation.

Sample	O	F	Na	Si	Ca	Fe	La	Ce	Total	
205_1_6	13.77	9.32	–	0.84	0.16	–	24.32	49.87	98.27	
205_1_7	12.94	10.98	0.34	0.64	0.16	–	31.26	38.67	94.98	
205_1_36	13.65	7.32	–	0.23	0.12	1.14	25.14	50.65	98.24	
205_1_37	12.01	21.94	0.76	0.30	0.26	1.11	60.41	3.21	100.00	
205_1_38	13.81	14.29	–	1.08	0.29	2.87	32.75	34.90	100.00	
205_1_82	14.16	9.01	0.46	0.59	0.29	2.04	33.94	39.50	100.00	
205_1_84	15.73	3.64	0.70	1.45	0.46	2.32	27.17	48.41	100.00	
205_1_100	13.38	11.16	0.46	0.20	0.12	1.86	30.47	41.71	99.37	
205_1_101	12.95	14.15	0.60	0.80	0.19	2.06	39.31	25.52	95.58	
205_1_102	13.79	18.41	–	2.68	0.13	4.14	36.24	18.89	94.28	
205_2_38	12.75	16.34	0.61	0.28	0.15	1.12	41.66	27.09	99.99	
205_2_96	14.36	9.85	–	1.78	0.22	1.42	35.76	33.05	96.43	
205_2_97	15.66	13.73	–	3.91	0.23	0.74	42.08	21.22	97.57	
205_2_103	13.59	10.96	–	0.62	0.31	2.05	28.72	42.08	98.34	
205_3_21	13.34	13.45	0.55	0.76	0.49	0.53	39.73	29.57	98.42	
205_3_23	13.86	7.67	1.14	0.63	0.60	0.61	21.77	50.02	96.30	
205_3_28	13.42	7.53	–	0.50	0.29	1.51	35.77	35.74	94.76	
205_4_16	13.42	12.35	0.45	0.25	0.22	1.95	37.56	34.12	100.33	
				Atom per formula unit						
205_1_6	1.237	1.763	–	0.053	0.007	–	0.310	0.630	4.000	
205_1_7	1.235	1.765	0.027	0.042	0.007	–	0.415	0.509	4.000	
205_1_36	1.576	1.424	–	0.014	0.005	0.036	0.315	0.630	4.000	
205_1_37	1.182	1.818	0.063	0.020	0.012	0.038	0.824	0.043	4.000	
205_1_38	1.603	1.397	–	0.066	0.012	0.088	0.405	0.428	4.000	
205_1_82	1.369	1.631	0.033	0.034	0.012	0.060	0.400	0.461	4.000	
205_1_84	2.093	0.907	0.045	0.076	0.017	0.061	0.289	0.511	4.000	
205_1_100	1.171	1.829	0.034	0.012	0.005	0.057	0.378	0.513	4.000	
205_1_101	0.985	2.015	0.046	0.051	0.008	0.066	0.504	0.324	4.000	
205_1_102	0.858	2.142	–	0.168	0.006	0.130	0.459	0.237	4.000	
205_2_38	0.883	2.117	0.048	0.018	0.007	0.036	0.542	0.349	4.000	
205_2_96	1.314	1.686	–	0.108	0.009	0.043	0.438	0.401	4.000	
205_2_97	1.136	1.864	–	0.227	0.009	0.022	0.495	0.247	4.000	
205_2_103	1.196	1.804	–	0.038	0.013	0.064	0.360	0.524	4.000	
205_3_21	1.039	1.961	0.042	0.047	0.021	0.017	0.502	0.370	4.000	
205_3_23	1.474	1.526	0.081	0.037	0.024	0.018	0.256	0.584	4.000	
205_3_28	1.463	1.537	–	0.032	0.013	0.048	0.456	0.452	4.000	
205_4_16	1.102	1.898	0.034	0.015	0.009	0.060	0.464	0.418	4.000	

Dash—content of an element below the accuracy of the test method.

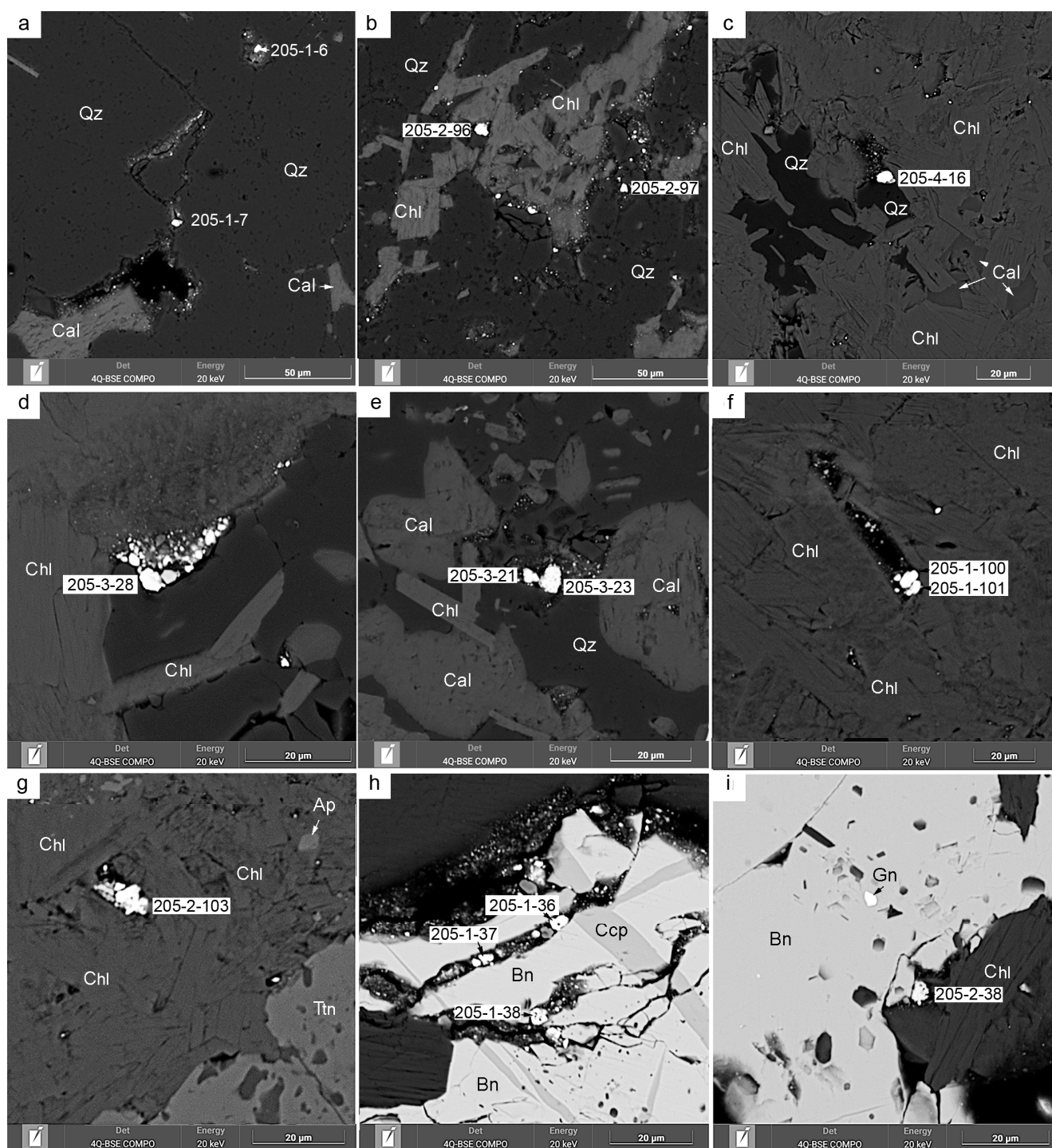


**Figure 4.** Microphotographs of oxyfluorides (a–i) in the rocks of the Shatak Formation. The numbers shown on the microphotographs correspond to the analysis numbers in Table 1. The abbreviations used are as follows: Chl—chlorite; Cal—calcite; Ttn—titanite; Ap—apatite; Qz—quartz; Bn—bornite; Ccp—chalcopyrite; and Gn—galena.

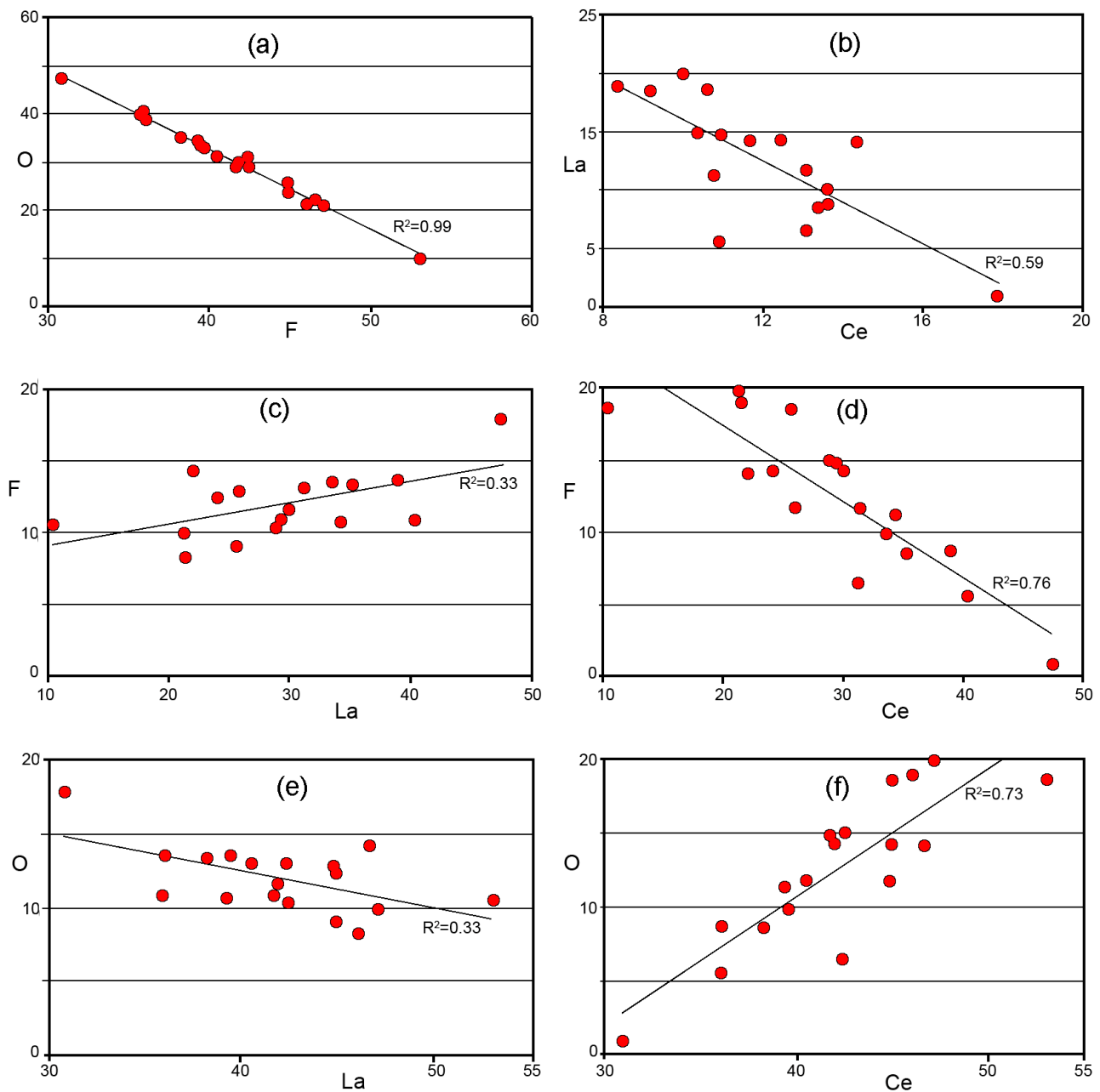


**Figure 5.** Binary phase diagrams (a–f) illustrating the elemental composition of oxyfluorides in rocks from the Shatak Formation, represented in atomic percentages (at. %). Detailed explanations regarding the diagrams can be found in the accompanying text.

The general formula for oxyfluorides can be expressed as  $(La, Ce)(O_nF_m)_3$ , where F/O and La/Ce ratios range from 0.433 to 2.498, and from 0.492 to 18.983, respectively. The stoichiometric composition of the identified oxyfluorides was influenced by the presence of mechanical impurities, such as Na, Si, Ca, and Fe, which can affect the calculations. In this case, the detected oxyfluorides exhibited cationic non-stoichiometry ranging from 0.06 to 0.304 f.c, respectively.

## 5. Discussion

The process of transitioning from rare-earth trifluorides to oxyfluorides has been extensively studied. In  $RF_3-R_2O_3$  systems, this transition occurs in three stages of  $F^{1-} \rightarrow O^{2-}$  replacement, which can be distinguished based on the oxygen content. The final stage

involves the complete substitution of fluorine with oxygen, resulting in the formation of oxides. In the intermediate stage, compounds such as ROF are formed, which have limited homogeneity areas [15]. When trifluorides are heated to temperatures ranging from 450 to 800 °C, they interact with the moisture present in the air, leading to the removal of hydrogen fluoride (HF) through a pyrohydrolysis reaction. Oxyfluorides formed as intermediate products during this reaction further transform into oxides upon their interaction with water vapor [14]. It is important to note that even small amounts of adsorbed moisture present in any powdered sample are sufficient for this process to occur.

Oxyfluorides can be produced from oxides through a direct solid-state reaction at temperatures below or equal to 650 °C [32]. Another method involves milling lanthanum oxide (La<sub>2</sub>O<sub>3</sub>) and lanthanum fluoride (LaF<sub>3</sub>), which leads to the formation of lanthanum oxyfluoride (LaOF) at room temperature through a mechanochemical reaction [33].

Therefore, during the formation of minerals in actual geological settings, a variety of mechanisms for oxyfluoride formation can occur under different physical and chemical conditions.

The presence of the microglobular structures of oxyfluorides within schlier-like segregations, which could potentially represent cavities, suggests that the formation of mineralization occurred through a metamorphogenic process. The rocks of the Shatak Formation underwent two distinct stages of metamorphism at different times. The first stage involved thermal (endocontact) metamorphism, which affected the quartz sandstones exposed to the flood basalts. The second stage corresponds to regional dynamothermal metamorphism, with the maximum thermobaric conditions reaching approximately T = 460 °C and P = 8 kbar [34]. By analyzing the temperatures required for chlorite formation in the rocks of the entire Shatak Formation, which were calculated based on the work of Kranidiotis et al. [35], it can be observed that the development of exocontact chlorite rocks, in which oxyfluoride mineralization was observed, was influenced by regional metamorphism. This observation is further supported by the fact that chlorites from rhyolites, metabasalts, and terrigenous deposits form a uniform field (Figure 6).

During the formation of the hydrothermal system, it is crucial to understand the sources of the main components of oxyfluorides, specifically fluorine, lanthanum, and cerium. Figure 3 shows a significantly higher fluorine content in the metabasalts as compared to the average content in similar rocks, which was around 681 ppm [36]. On the other hand, the fluorine content in the terrigenous rocks and rhyolites was comparable to the average content in similar formations, such as acid volcanic rocks (846 ppm) and sandstones (485.5 ppm) [36]. Most of the fluorine is incorporated into fluorapatite, which is unstable under hydrothermal metamorphism conditions [37,38], as well as during hypergenesis [39]. Additionally, rare-earth elements (wt%) were detected in the composition of fluorapatite from terrigenous rocks. The lanthanum (La) content ranged from 0.68 to 1.57, cerium (Ce) from 1.42 to 2.83, and neodymium (Nd) from 0.49 to 0.8, respectively.

The extent of hydrothermally altered rocks within this section and the potential migration of rare-earth elements and fluorine, leading to their redeposition and concentration on geochemical barriers, are illustrated in Figure 7. Shale clasts undergo a process of “pseudomorph” replacement, characterized by the presence of lanthanum, cerium, neodymium, allanite, and fluorapatite microaggregates. While the formation of rare-earth trifluorides is generally impeded under the conditions of excess oxygen resulting from water dissociation, there is still a possibility for their formation through the mechanism proposed by A.C. Strzelecki et al. [11]. The differences in the chemical composition of oxyfluorides formed under these conditions can be attributed, in our opinion, to local variations in the content of the main components (O, F, Ce, and La) within the forming microcracks.

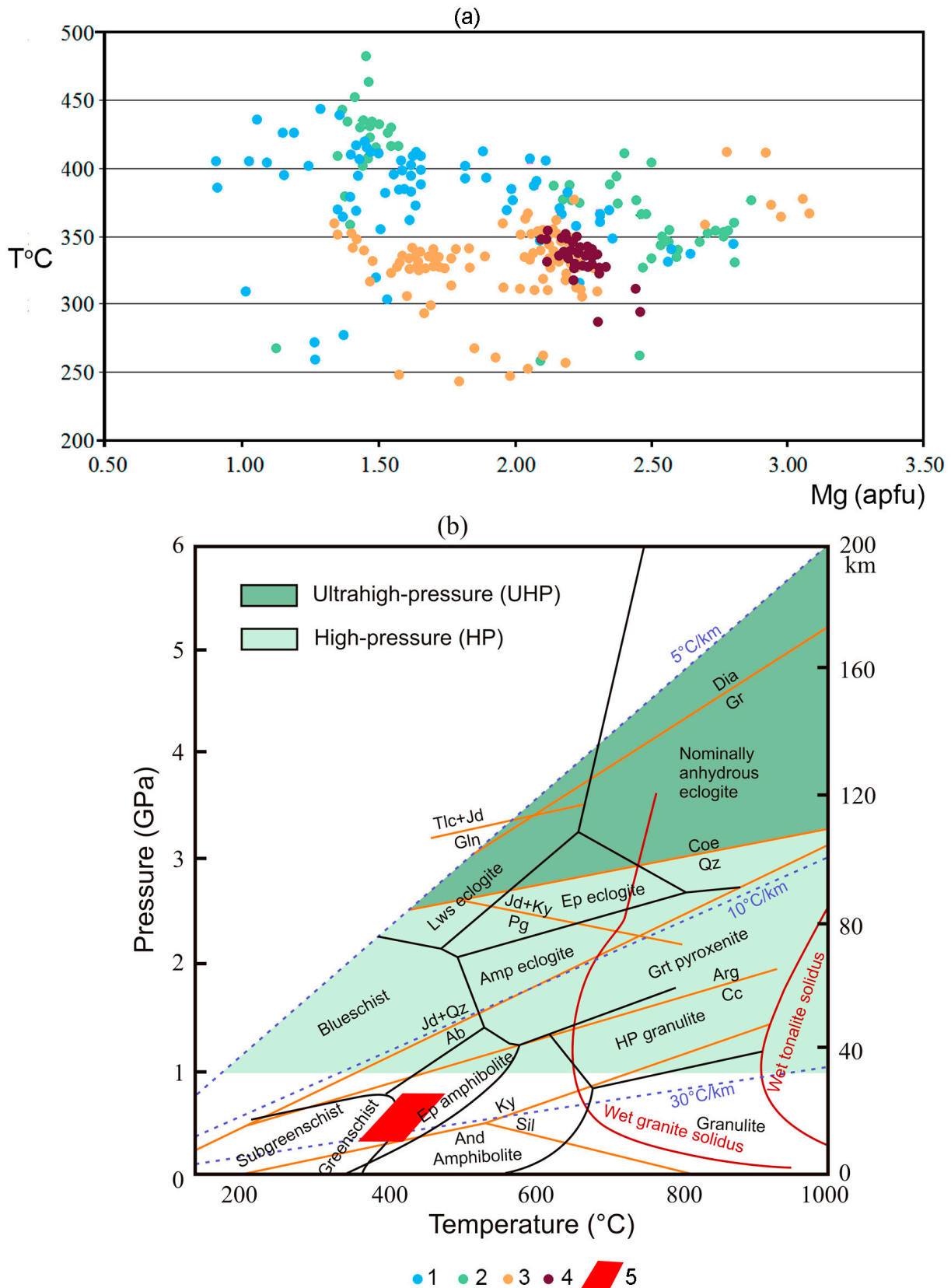


**Figure 6.** (a) T°C—Mg (apfu) diagram for chlorites from rocks of the Kuz'elga Sub-formation of the Shatak Formation. (b) P—T diagram for light micas from rocks of the Shatak Complex by [40]. 1—terrigenous rocks; 2—metabasalts; 3—rhyolites; 4—contact rocks; and 5—thermobaric parameters for light micas from rocks of the Shatak Complex.

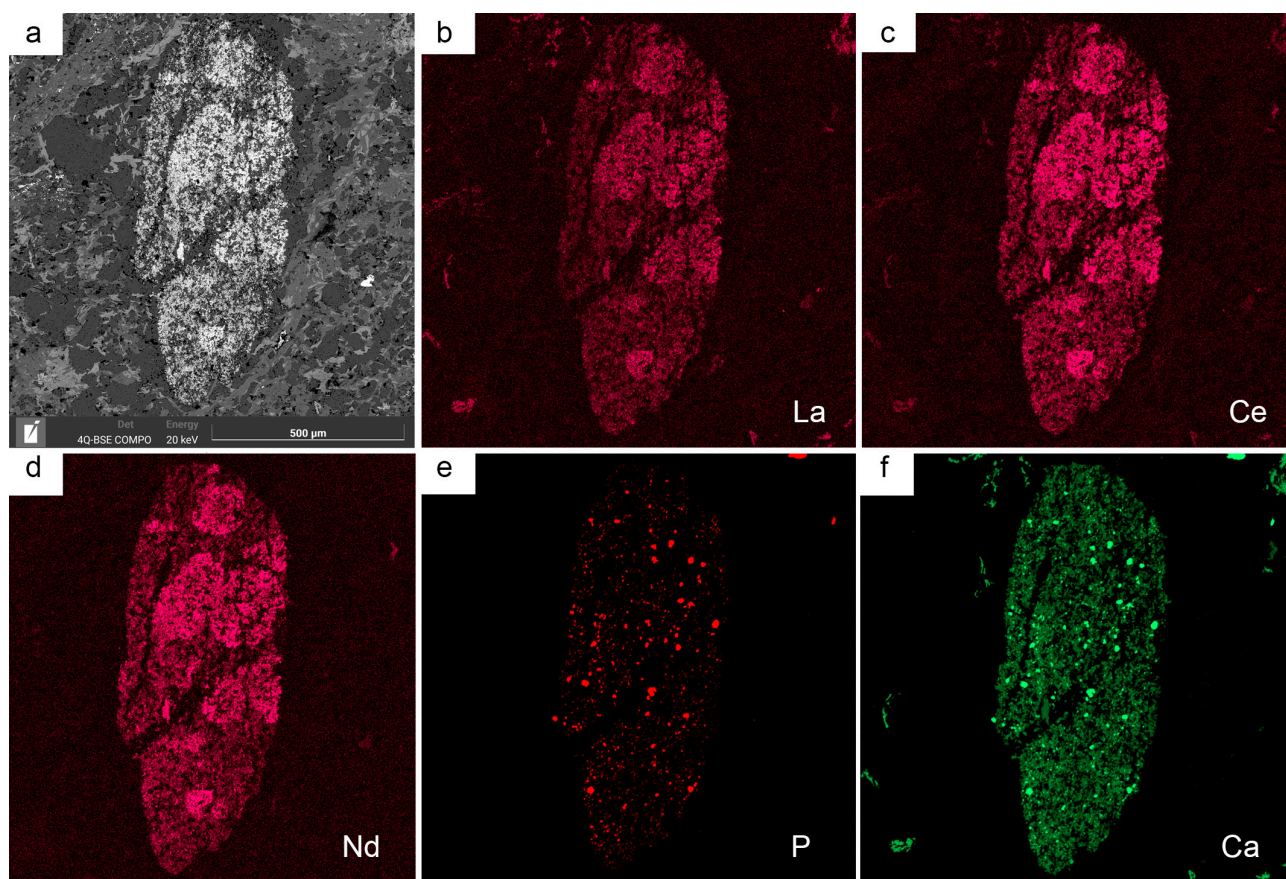


**Figure 7.** Microphotograph of a shale clast showing pseudomorphic substitution by an assemblage of rare-earth elements, as well as allanite and fluorapatite (a–f).

## 6. Conclusions

1. Oxyfluoride (La, Ce)  $(O_nF_m)_3$  mineralization, represented by compounds of variable composition forming an isomorphic series, is described for the first time in the volcanogenic–sedimentary rocks of the Shatak Complex: trifluoride, (La, Ce) $F_3$ –oxyfluoride, (La, Ce)OF–oxide, and (La, Ce) $_2O_3$ . Analysis of various binary phase diagrams revealed a strong correlation between oxygen, fluorine, and cerium in the chemical composition of oxyfluorides, while the behavior of lanthanum showed more unsystematic tendencies;
2. The origin of oxyfluoride mineralization in the Shatak Formation can be attributed to the regional metamorphism of rocks. The hydrothermal process involves the decomposition of fluorapatite, which is unstable during both hydrothermal metamorphism and hypergenesis, resulting in the release of fluorine, as well as potentially lanthanum and cerium. Variations in the chemical composition of oxyfluorides formed under the conditions of excess oxygen due to water dissociation can be attributed to local variations in the concentrations of the main components within the developing microcracks.

**Author Contributions:** S.G.K., S.S.K. and A.A.S. contributed to the investigation, field work, and sample preparation; S.G.K. and A.A.S. contributed to the writing of the original draft; S.G.K. contributed to the writing, review and editing of the manuscript; S.S.K. conducted the study of samples on an electron microscope; S.G.K. was involved in project administration; S.G.K., S.S.K. and A.A.S. acquired funding for the study. All authors have read and agreed to the published version of the manuscript.

**Funding:** This study was supported by the Russian Science Foundation grant No. 23-27-00023.

**Data Availability Statement:** The data presented in this study are available upon request from the corresponding author.

**Conflicts of Interest:** The authors declare no conflict of interest.

## References

1. Heinrich, E.W.M.; Gross, E.B. Fluocerite and associated minerals from the Black Cloud pegmatite, Teller County, Colorado. *Am. Mineral.* **1960**, *45*, 455–459.
2. Feldman, L.G.; Surkov, B.K.; Stolyarova, T.I. Fluocerite from rare-metal granites of the northern Tien Shan and some data on the genetic mineralogy of fluorides of rare earth elements. *Tr. Mineral. Muzeja Im. A. E. Fersmana AN SSSR* **1973**, *22*, 143–157. (In Russian)
3. Wambeke, L.V. The Karonge rare earth deposits, Republic of Burundi: New mineralogical-geochemical data and origin of the mineralization. *Miner. Depos.* **1977**, *12*, 373–380. [[CrossRef](#)]
4. Lahti, S.I.; Suominen, V.I. Occurrence, crystallography and chemistry of the fluocerite-bastnaesite-cerianite intergrowth from the Fjalskar granite, southwestern Finland. *Bull. Geol. Soc. Finl.* **1988**, *60*, 45–53. [[CrossRef](#)]
5. Beukes, G.J.; Bruyn, H.D.; Westhuizen, W.A. Fluocerite and associated minerals from the Bavianskranz granite pegmatite near Kakamas, South Africa. *S. Afr. J. Geol.* **1991**, *94*, 313–320.
6. Williams-Jones, A.E.; Migdisov, A.A.; Samson, I.M. Hydrothermal Mobilisation of the Rare Earth Elements—A Tale of “Ceria” and “Yttria”. *Elements* **2012**, *8*, 355–360. [[CrossRef](#)]
7. Borisova, E.B.; Ivanova, A.A.; Badanina, E.V. Features of accessory Li–F mineralization of amazonite granites of the Turga massif in Eastern Transbaikalia. *Trudy Kol'skogo nauchnogo tsentra RAN. Geol. i Geokhim.* **2019**, *1*, 52–56. (In Russian)
8. Starikova, A.E.; Sklyarov, E.V.; Sharygin, V.V. Y–REE Mineralization in Biotite–Arfvedsonite Granites of the Katugin Rare-Metal Deposit, Transbaikalia, Russia. *Dokl. Earth Sci.* **2019**, *487*, 800–803. Available online: <https://link.springer.com/article/10.1134/S1028334X19070080> (accessed on 23 August 2019). [[CrossRef](#)]
9. Raschke, M.B.; Stern, C.R.; Anderson, E.J.D.; Skewes, M.A.; Farmer, G.L.; Allaz, J.M.; Persson, P.M. Bulk composition of a zoned rare-earth minerals-bearing pegmatite in the Pikes Peak granite batholith near Wellington Lake, central Colorado, U.S.A. *Rocky Mt. Geol.* **2021**, *56*, 1–18. [[CrossRef](#)]
10. Gorelikova, N.V.; Semenyak, B.I.; Korostelev, P.G.; Taskaev, V.I.; Balashov, F.V.; Rassulov, V.A. Rare earth minerals in rare-metal greisens of the Verkhnee deposit (Khingano-Olonoiysky district, Amur region, Russia). *Tikhookeanskaya Geol.* **2022**, *41*, 75–91. [[CrossRef](#)]
11. Strzelecki, A.C.; Migdisov, A.; Boukhalfa, H.; Sauer, K.; McIntosh, K.G.; Currier, R.P.; Williams-Jones, A.E.; Guo, X. Fluocerite as a precursor to rare earth element fractionation in ore-forming systems. *Nat. Geosci.* **2022**, *15*, 327–333. [[CrossRef](#)]
12. Rowland, R.L.; Lavina, B.; Van der Kaaden, K.E.; Danielson, L.R.; Burnley, P.C. Thermal Analysis, Compressibility, and Decomposition of Synthetic Bastnäsite-(La) to Lanthanum Oxyfluoride. *Minerals* **2020**, *10*, 212. [[CrossRef](#)]
13. Zhang, W.; Chen, W.T.; Williams-Jones, A.E. An unique, fluocerite-rich REE deposit in Henan province, Central China: The missing link in magmatic-hydrothermal REE mineralizing systems? *Contrib. Mineral. Petrol.* **2023**, *178*, 34. [[CrossRef](#)]
14. Batsanova, L.R. Fluorides of rare earth elements. *Uspekhi Khimii AN SSSR* **1971**, *6*, 945–979. (In Russian)
15. Sobolev, B.P. Nonstoichiometry in Inorganic Fluorides. IV: *The Initial Stage of Anionic Nonstoichiometry in RF3 (R = Y, La, Ln)*. *Crystallogr. Rep.* **2021**, *66*, 349–360. (In Russian)
16. Holtstam, D.; Grins, J.; Nysten, P. Håleniusite-(La) from the Bastnäs deposit, Västmanland, Sweden: A new REE Oxyfluoride mineral species. *Can. Mineral.* **2004**, *42*, 1097–1103. [[CrossRef](#)]
17. Kampf, A.R.; Ma, C.; Chiappino, L. Håleniusite-(Ce), CeOF, the Ce Analogue of Håleniusite-(La) from the Água de Pau Volcano, São Miguel Island, Azores District, Portuga. *Can. Mineral.* **2022**, *60*, 713–717. [[CrossRef](#)]
18. Parnachev, V.P.; Rotar, A.F.; Rotar, Z.M. *Middle Riphean Volcanogenic-Sedimentary Association of the Bashkir Meganticlinorium (Southern Urals)*; UNC AN USSR: Sverdlovsk, Russia, 1986; 105p. (In Russian)
19. Puchkov, V.N. *Paleogeodynamics of the Southern and Middle Urals*; Dauria: Ufa, Russia, 2000; 146p. (In Russian)
20. Puchkov, V.N. *Geology of the Urals and Cis-Urals (Topical Issues of Stratigraphy, Tectonics, Geodynamics and Metallogeny)*; DesignPoligraphService: Ufa, Russia, 2010; 280p. (In Russian)
21. Maslov, A.V.; Krupenin, M.T.; Ronkin, Y.u.L.; Gareev, E.Z.; Lepikhina, O.P.; Popova, O.Y. Fine-grained aluminosiliciclastic formations of the Middle Riphean stratotype section in the Southern Urals: Features of formation, composition and evolution of provenances. *Lithol. Miner. Resour.* **2004**, *4*, 414–441. (In Russian)
22. Maslov, A.V.; Gareev, E.Z.; Podkovyrov, V.N.; Kovalev, S.G.; Kotova, L.N. Synrift sedimentary formations of the Mashak Formation of the Middle Riphean of the Southern Urals (brief lithochemical characteristics). *Bull. St. Petersburg State Univ. Earth Sci.* **2018**, *63*, 303–325. (In Russian)
23. Kovalev, S.G.; Vysotsky, I.V. A new type of noble metal mineralization in terrigenous rocks of the Shatak graben (western slope of the Southern Urals). *Lithol. Miner. Resour.* **2006**, *4*, 415–421. (In Russian) [[CrossRef](#)]
24. Kovalev, S.G.; Vysotsky, I.V. New data on the geology of the Shatak complex (western slope of the Southern Urals). *Lithol. Miner. Resour.* **2008**, *3*, 280–289. (In Russian) [[CrossRef](#)]
25. Kovalev, S.G.; Kovalev, S.S.; Vysotsky, S.I. Th–REE mineralization in Precambrian rocks of the Bashkir meganticlinorium: Species diversity and genesis. *Geol. Ore Depos.* **2017**, *5*, 59–79.
26. Puchkov, V.N.; Krasnobaev, A.A.; Sergeeva, N.D. The New Data on Stratigraphy of the Riphean Stratotype in the Southern Urals, Russia. *J. Geosci. Environ. Prot.* **2014**, *2*, 108–116. [[CrossRef](#)]

27. McDonough, W.F.; Sun, S.S. Composition of the Earth. *Chem. Geol.* **1995**, *120*, 223–253. [[CrossRef](#)]
28. Rudnick, R.L.; Gao, S. Composition of the Continental Crust. *Treatise Geochem.* **2003**, *3*, 1–64.
29. Kovalev, S.G.; Vysotsky, S.I.; Kovalev, S.S.; Kotlyarov, V.A. Sulfide-selenide mineralization in volcanic-sedimentary rocks of the Shatak complex (Bashkir meganticlinorium). *Vestnik IG Komi NTs UrO RAN* **2017**, *7*, 21–27. (In Russian) [[CrossRef](#)]
30. Bulakh, A.G. *Guidelines and Tables for Calculating Mineral Formulas*; Nedra: Moscow, Russia, 1967; 141p. (In Russian)
31. Krivovichev, V.G.; Gulbin, Y.L. Recommendations for mineral formula calculations from chemical analytical data. *Zap. Ross. Mineral. Obs.* **2022**, *151*, 114–124. (In Russian)
32. Dutton, S.E.; Hirai, D.; Cava, R.J. Low temperature synthesis of LnOF rare-earth oxyfluorides through reaction of the oxides with PTFE. *Mater. Res. Bull.* **2012**, *47*, 714–718. [[CrossRef](#)]
33. Lee, J.; Zhang, Q.; Saito, F. Mechanochemical Synthesis of Lanthanum Oxyfluoride from Lanthanum Oxide and Lanthanum Fluoride. *J. Am. Ceram. Soc.* **2004**, *84*, 863–865. [[CrossRef](#)]
34. Kovalev, S.S.; Puchkov, V.N.; Kovalev, S.G.; Vysotsky, S.I. The First Quantitative Evaluation Data on Vendian Metamorphism in the Eastern Part of the Bashkir Meganticlinorium. *Dokl. Earth Sci.* **2018**, *483*, 1418–1422. [[CrossRef](#)]
35. Kranidiotis, P.; MacLean, W.H. Systematic of chlorite alteration at the Phelps Dodge massive sulfide deposit, Matagami, Quebec. *Econ. Geol.* **1987**, *82*, 1808–1911. [[CrossRef](#)]
36. Koga, K.T.; Rose-Koga, E.F. Fluorine in the Earth and the solar system, where does it come from and can it be found? *Comptes Rendus Chim.* **2018**, *21*, 749–756. [[CrossRef](#)]
37. Harlov, D.E. Apatite: A Fingerprint for Metasomatic Processes. *Elements* **2015**, *11*, 171–176. [[CrossRef](#)]
38. Broom-Fendley, S.; Styles, M.T.; Appleton, J.D.; Gunn, G.; Wall, F. Evidence for dissolution-reprecipitation of apatite and preferential LREE mobility in carbonatite-derived late-stage hydrothermal processes. *Am. Mineral.* **2016**, *101*, 596–611. [[CrossRef](#)]
39. El Agami, N.L.; Abd El Wahed, A.A.; Haroun, Y.S. Apatite alteration and its relation to REE fractionation and u-mineralization, a case study of Western Desert and Sinai, Egypt. In Proceedings of the 4th International Conference on the Geology of Africa, Addis Ababa, Ethiopia, 4–7 February 2005; Volume 1, pp. 131–153.
40. Zheng, Y.F.; Chen, R.X. Regional metamorphism at extreme conditions: Implications for orogeny at convergent plate margins. *J. Asian Earth Sci.* **2017**, *145*, 46–73. [[CrossRef](#)]

**Disclaimer/Publisher’s Note:** The statements, opinions and data contained in all publications are solely those of the individual author(s) and contributor(s) and not of MDPI and/or the editor(s). MDPI and/or the editor(s) disclaim responsibility for any injury to people or property resulting from any ideas, methods, instructions or products referred to in the content.